Nuclear Instruments and Methods in Physics Research A241 (1985) 62–71
North-Holland, Amsterdam

A STUDY OF IONIZATION ELECTRONS DRIFTING LARGE DISTANCES IN LIQUID AND SOLID ARGON

E. APRILE, K.L. GIBONI and C. RUBBIA

High Energy Physics Laboratory, Harvard University, Cambridge, MA 02138, USA

Received 5 June 1985

A two liter gridded ionization chamber was built and operated repeatedly to study electron transport in liquid and solid argon over distances up to 10 cm in drift fields of 0.01–2 kV/cm. A detailed analysis of the ionization pulse shape was performed, yielding information on both the degree of purity of the liquid and the electron drift velocity. Argon with an impurity concentration less than 0.2 ppb oxygen equivalent was obtained with a simple purification system. The measured attenuation length extrapolates to 7.5 m for liquid argon and to 1 m for solid argon at a drift field of 1 kV/cm.

1. Introduction

Cryogenic liquids and solids rather than gases have been known for a long time to represent ideal media for a continuously sensitive image chamber device. The high density and the excellent spatial and energy resolution make this novel type of detector especially suited for the first direct observation of solar neutrinos, by the recoil electrons from the ν_e e scattering. The possibility of a precise determination of the neutrino direction of incidence is extremely important as it permits to correlate the effect to the position of the sun, and it insures a convincing subtraction of other backgrounds. This is a clear advantage over solar neutrino experiments based on the radiochemical technique [1].

Equally important are the advantages that such a device would bring in the search for proton decay. Due to the tracking capability and the high resolution of the drift chamber, proton decay modes have an unambiguous signature and can be much more easily separated from the background of neutrino induced reactions. The limitations of the present generation of large proton decay experiments, namely the limited vertex, energy and tracking resolutions in the presence of neutrino backgrounds, can be easily overcome.

The principal challenge for the realization of a large volume cryogenic image chamber device is to achieve long drift distances of the ionization electrons, at relatively moderate electric fields. Due to attachment of free electrons to electronegative impurities, mainly oxygen [2], long drift distances imply very low impurity concentrations (less than one part per billion of oxygen equivalent). Since the initial proposal in 1977 of a liquid argon drift chamber [3] a large amount of work has been carried out in order to ascertain the feasibility of the method and in particular in order to develop the technology of attaining the degree of purity necessary to drift electrons over several meters in liquid argon [4–9].

The possibility of using solid rather than liquid argon has been less throughly investigated [10]. The solid phase offers the advantage of a higher electron mobility [11] and, more importantly, it can be safer when operating a large volume cryogenic detector in an underground laboratory. Additionally a solid argon detector is less sensitive to mechanical vibrations and to impurity leaks [12].

2. Chamber design

A schematic view of the test detector is shown in fig. 1. Two discs at a distance of 10 cm formed the cathode and the anode of a gridded ionization chamber. The screening grid was mounted in the drift space 4 mm from the anode. The uniformity of the field was ensured by five field shaping rings positioned equidistantly, enclosing the active volume. On the other side of the anode an additional disc was mounted at a distance of 1.4 cm. By applying HV to this disc in place of the cathode, a simple ionization chamber was available to study electron transport at higher electric fields.

All the electrodes and the field shaping rings were made from stainless steel, held in place by ceramic spacers. The screening grid consisted of 50 μm BeCu wires spaced by 1 mm. They were soldered to an Inconel ring which served as grid-frame. The grid had a shielding efficiency of 95% and was totally transparent to electron drifting, if the electric field between the anode and the grid was at least 1.5 times stronger than the drift field between the cathode and the grid [13]. The

0168-9002/85/$03.30

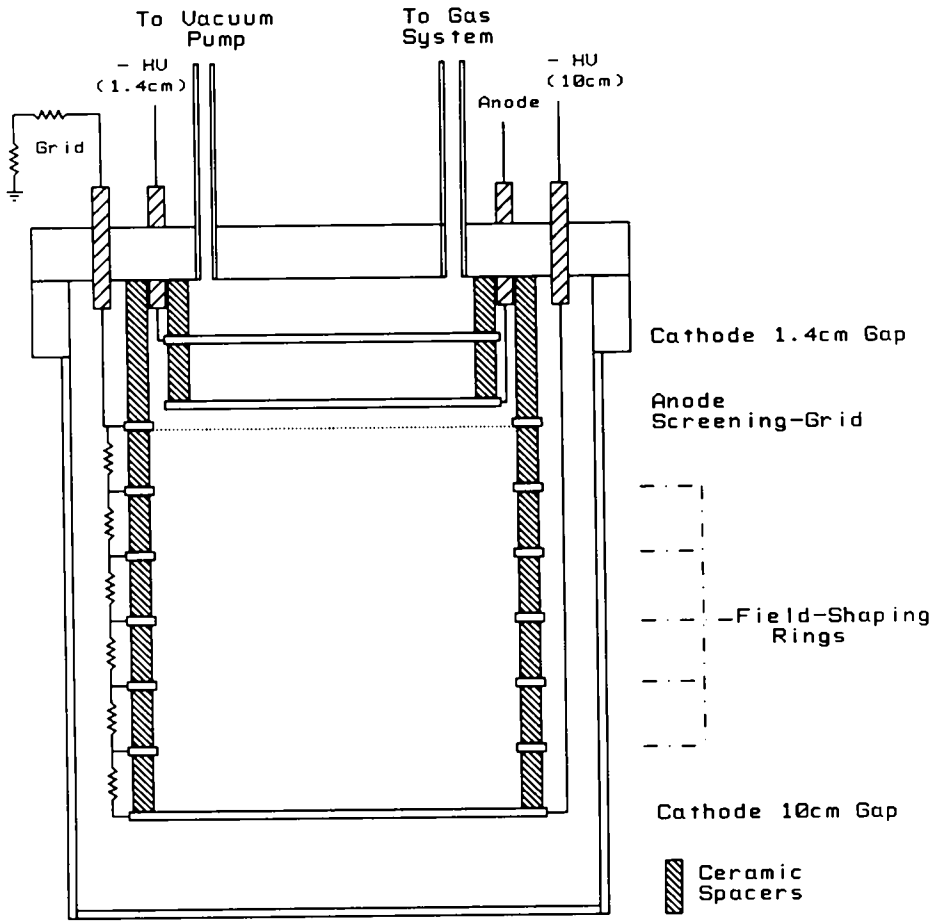

Fig. 1. Schematic cross section of the test chamber.

resistors of the HV chain were mounted directly on the field shaping rings, to keep the number of electrical feedthroughs small. The resistor from the grid to ground was outside the chamber to allow an adjustment of the grid-anode field strength. This assembly was mounted in a stainless steel container of 13 cm diameter and 15 cm height. The container was closed on the top by a steel flange from which the chamber was suspended. Two 1/4 in. gas supply lines and 6 HV feed-throughs were welded on the top flange. An indium wire was used to seal the flange to the container. This guarantied a leak tight chamber with leak rates smaller than 10^{-8} Torr l s^{-1}, even after cooling to liquid argon temperature. Due to this small leak rate, the chamber could be disconnected from the vacuum pump with an pressure rise of less then 10^{-3} Torr (the sensivity of the gauge) after about 40 h. This allowed to operate the detector for at least 2 d without seriously affecting the purity of the liquid. A metal film resistor served as level detector to indicate that the chamber was completely filled with the liquid.

3. Gas purification system

A schematic drawing of the gas purification system is shown in fig. 2. It was designed to be easily expandable for future large-scale applications. Commercially available argon gas with an impurity level of < 1 ppm oxygen and < 5 ppm nitrogen, was first passed through an Oxisorb cartridge [14] to remove the bulk of the oxygen concentration. The resulting argon should contain less than 10 ppb oxygen equivalent. The gas was subsequently filtered through two molecular sieves, a 13X and a 4A type [15], to further reduce the oxygen level and to remove other impurities. The 4A molecular sieve was kept at dry ice temperature. The volume of each sieve was 0.9 l.

The gas system was made of stainless steel tubing. To avoid leaks, the tubes were either welded or connected with good vacuum fittings [16]. Bellow valves were used to minimize the possibility of air entering the system. Before assembly all parts of the gas system were carefully cleaned. The closed system was then kept

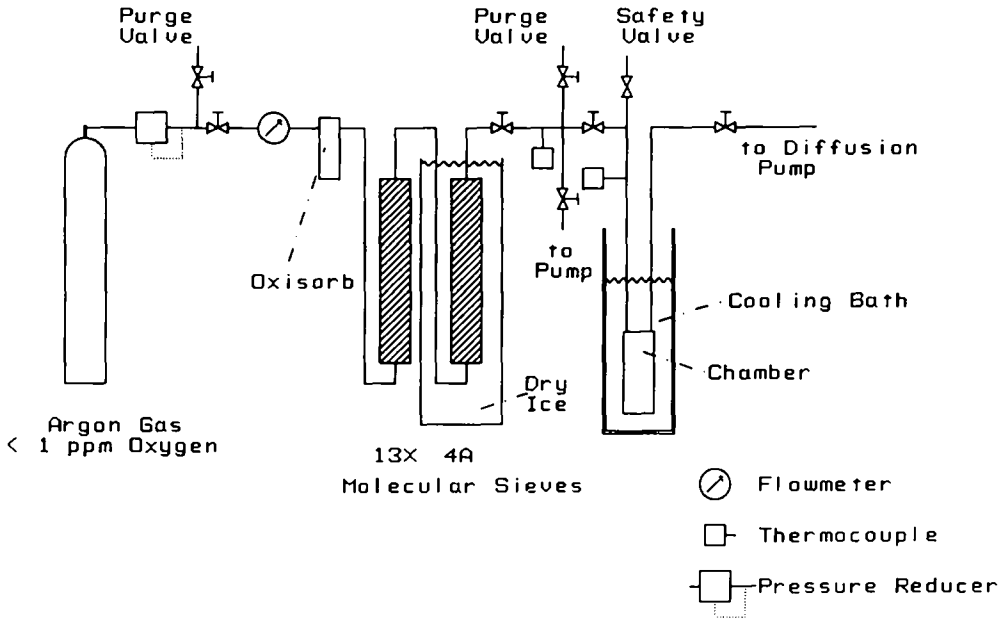

Fig. 2. Lay-out of the gas system.

under vacuum for at least 24 h to reduce out-gassing from the walls. The molecular sieves were baked-out under vacuum at 220°C.

After purification as described above the argon gas was liquefied in the chamber. For the measurements with liquid argon the test chamber was cooled by a bath of liquid argon. For the tests with solid argon a bath of liquid nitrogen was used. As an open dewar was used, the level of the cooling liquid could be easily controlled. Changing the cooling bath from argon to nitrogen and back also presented no problem. The use of an open dewar represented the easiest and simplest solution for a small test set-up, without the need of a liquid handling and control system.

Filling of the chamber with liquid argon took about 2.5 h. The flow rate of about 180 cm^3/s was mainly determined by the heat transfer through the chamber walls.

4. Data-taking

After filling the chamber with liquid argon the valve to the gas system was closed. Cosmic rays penetrating the chamber were used as ionizing particles. When sufficient data were recorded with the liquid, the cooling bath was changed from liquid argon to liquid nitrogen, to pass to the measurements with the solid. The argon in the chamber started to freeze. Several hours were allowed for this process to complete. After data-taking with the solid the bath was changed back to liquid argon, in order to verify that the impurity level did not vary considerably. The cooling bath was then finally removed and the argon in the chamber was allowed to evaporate through the purge valve. With this sequence a typical run lasted more than 48 h. Several runs were successfully performed, proving the reliability of the detector.

During data taking all vacuum pumps were turned off to diminish the effect of vibrations. Mechanical vibrations showed up on the anode signal as superimposed oscillations with the mechanical resonance frequency of the chamber assembly. This kind of noise did not pose a serious problem, as the frequency was normally much lower than the signals. It could be observed as a baseline shift on the pulses. At the longest drift times observed (1.8 ms) a clear separation of signals and noise was still possible, as the recorded pulse shapes are vastly different. The microphony effect was strongly reduced in the solid argon.

5. Readout system

The anode signals from cosmic ray particles traversing the sensitive volume were fed into a charge sensitive preamplifier. The input stage was the standard circuit with a FET [17] in complementary cascode. As the HV was supplied to the cathode of the chamber, the anode was at ground potential. The gate of the FET could be directly connected to the anode without any coupling capacitor. To obtain a better matching be-

tween the capacitance of the chamber and the input capacitance of the amplifier, the FET and the feedback network were mounted on the chamber, i.e. within the liquid bath (see also ref. [4]). Two coaxial cables connected the FET and the feedback network with the rest of the amplifier outside the liquid at a distance of about 0.5 m. The amplifier incorporated no pulse shaping. The integration time constant of the input stage was set to 4 ms in order to observe even long drift-times without significant distortions. The input stage was followed by two stages to increase the output voltage and a line driver.

The amplified pulses were large enough to be fed directly into a wave form digitizer. The digitizer was built up with a 30 MHz 6 bit FADC, a memory for up to 2048 points, a software controllable clock, and a trigger circuit. The maximum clock frequency was 5 MHz, limited by the memory. During data acquisition the FADC was digitizing continuously and only stopped a software-controllable amount of time after a trigger. Thus it was possible to record the complete pulse, beginning even before arrival of the trigger.

The trigger was generated either by a triple coincidence of scintillation counters sandwiching the chamber or was derived by a discriminator from the chamber pulses itself.

The memory of the wave form digitizer was read out via CAMAC into a Super-Caviar processor. Here the data could be viewed online and passed on to a Vax 11/780 for recording. The tests of the whole readout chain and the calibration were achieved by test-pulses coupled with a 1 pF capacitor to the gate of the FET in the input stage.

The noise level was measured to be about 0.15 fC, where the noise was reduced in absence of a pulse shaping network by observing the pulse form and fitting an expected curve.

6. Pulse-shape analysis

The application of a wave-form digitizer allows one to study each ionization signal and to compare it with the expected pulse shape. More information is available than by only measuring the collected charge. The charge, the drift-time, and the attenuation of the signal by attachment of electrons to impurities can be determined for each pulse, independent of the amount of ionization which each particle produces. A particle traversing both gaps (the gridded 10 cm chamber and the simple 1.4 cm gap) produces different pulse shapes depending on which cathode was supplied with HV. In the 10 cm chamber the ionization electrons are accelerated by the field between cathode and grid. The anode can see the drift-

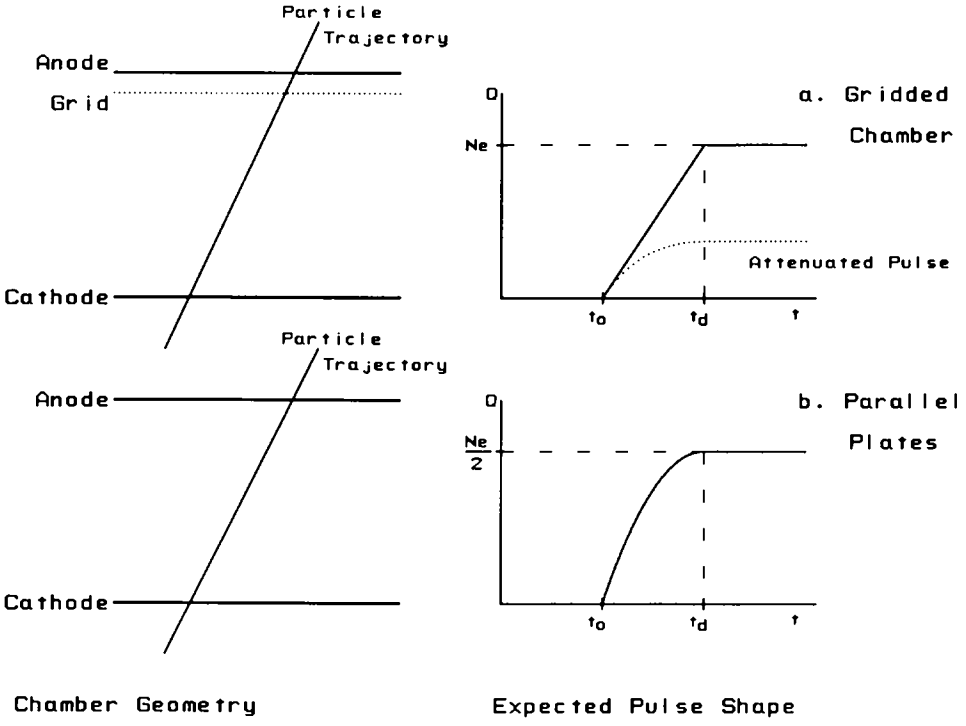

Fig. 3. Expected pulse shapes for particles passing through the two different types of electrode arrangement: the gridded chamber and the parallel plate chamber.

ing electrons only once they passed the grid. Thus the output signal for a straight track rises linearly with time, until all charges are collected. If impurities are present, the linear rise is modified by an exponential term which accounts for the effect of attachment (fig. 3a). The expected pulse shape is therefore:

$$Q(t) = Ne\frac{t}{t_d}\exp(-t/\tau), \qquad (1)$$

where Ne is the charge left in the drift space after initial recombination has taken place, t_d is the total drift time, and τ is the decay constant corresponding to the attenuation length divided by drift velocity.

For the 1.4 cm chamber all charges left between cathode and anode induce a signal when they are moved in the electric field. The resulting pulse shape (fig. 3b) is

$$Q(t) = Ne\left(\frac{t}{t_d} - \frac{1}{2}\left(\frac{t}{t_d}\right)^2\right), \qquad (2)$$

with Ne again the total charge and t_d the drift-time for the full drift space. Impurity attachment would contribute again with an exponential, but as the length of the gap is only 1.4 cm and the impurity concentration is small this term can be neglected.

The curves of eqs. (1) and (2) are fitted to each individual pulse. The charge, the total drift time, and the attenuation time are thus determined. This shows the full capability of a liquid argon chamber with a FADC readout. Particles traversing the entire chamber generate pulses which have the same drift time and attenuation time constant, at any given field strength. It is therefore possible to add up the pulses for each high voltage setting, to produce an "average pulse" which does not show the fluctuations of the single pulses. The characteristic values of these average pulses are the same as the ones determined from the distributions of the fits for single pulses. The development of the pulse shape at different drift fields can be more easily judged by comparing these average pulses.

7. Results

7.1. Liquid

The observed pulse shapes agree perfectly with the curves predicted by eqs. (1) and (2). Fig. 4 shows two typical pulses at two different field strengths (200 and 10 V/cm) for the 10 cm chamber. The fits of eq. (1) to the data points are superimposed. Fig. 5 shows the average of about 100 pulses for different field strengths in the 10 cm chamber. The effect of attachment to impurties can clearly be recognized from the increasing rounding of the pulses as the drift times grow longer with decreasing field strength. Fig. 6 gives the averages in the small gap for different fields. The pulse shape

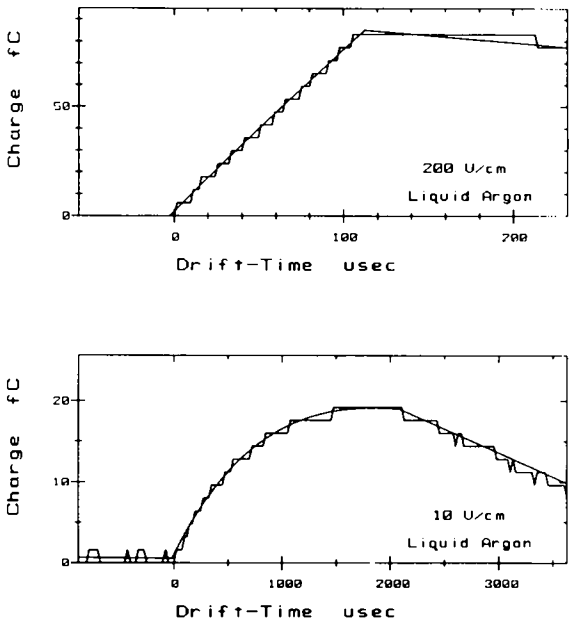

Fig. 4. Typical pulses in liquid argon for field strengths of 200 and 10 V/cm. The fit of the expected pulse shape is superimposed to the measured pulse form. The decay of the pulse at 10 V/cm is caused by the 4 ms integration time of the amplifier.

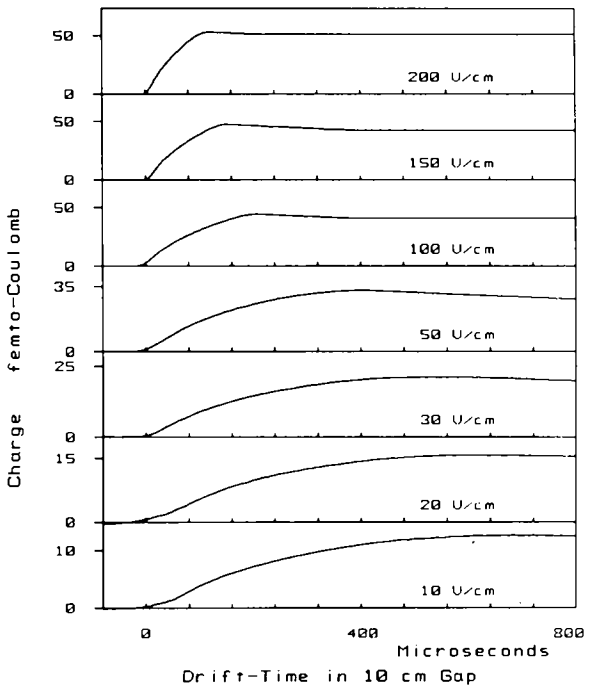

Fig. 5. Development of pulse shapes (average pulses) at different drift fields in the 10 cm chamber for liquid argon.

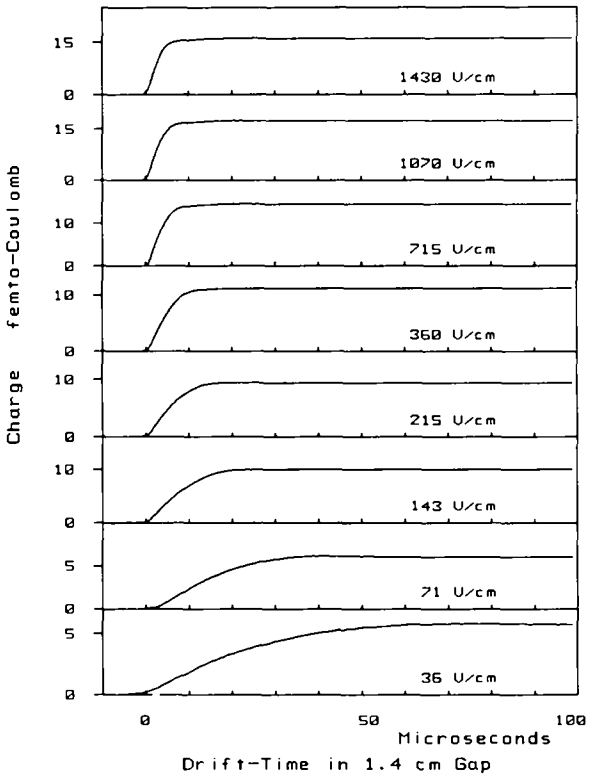

Fig. 6. Development of pulse shapes (average pulses) at different drift fields in the 1.4 cm chamber for liquid argon.

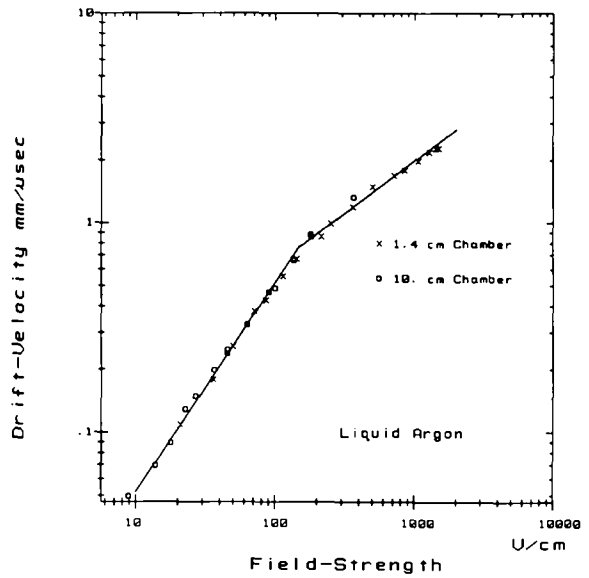

Fig. 7. Electron drift velocity in liquid argon versus field strength. The open circles represent the data points measured with the 10 cm chamber. The crosses are measured with the 1.4 cm gap. The solid line is a fit of a straight line up to 150 V/cm and a $E^{1/2}$ dependence thereafter.

Table 1
Measured drift velocities and electron mobilities in liquid argon in dependence of the electric field strength

E [V/cm]	v_d [mm/μs]	μ_0 [cm^2 s^{-1} V^{-1}]
1500	2.3	
1430	2.3	
1286	2.2	
1070	2.0	
857	1.8	
715	1.7	
500	1.5	
360	1.2	
250	1.0	
215	0.87	
184	0.87	
182	0.88	
143	0.68	476
138	0.67	486
137	0.67	489
114	0.56	491
101	0.49	485
91	0.47	517
86	0.43	500
64	0.33	516
50	0.26	520
46	0.25	544
37	0.20	541
36	0.18	500
27	0.15	548
23	0.13	565
21	0.11	524
18	0.091	508
14	0.073	519
9	0.051	562

stays the same only pulse height and rise time change.

From these curves the drift velocity can be directly determined as the drift distance is known. For the large gap this is only true until the attenuation length gets smaller than the length of the chamber of 10 cm. From the pulse shape one can decide whether this is the case. If the attenuation length is larger than the chamber dimension, the curve shows a distinct kink when charge collection is finished. For smaller attenuation lengths the curve smoothly reaches a constant value at the end of charge collection. The measured drift velocity in function of the applied field is shown in fig. 7 for the liquid. Up to about 150 V/cm the drift velocity follows a straight line, with the electron mobility as slope and zero intercept. Thereafter the data points can be represented by the function $v_d = c\mu_0 E^{1/2}$. The fit is represented by a solid line in fig. 7. The electron mobility is determined to be (516 ± 27) cm^2 s^{-1} V^{-1}. The best value for c is 0.00383 ± 0.00014. Table 1 lists the measured drift velocities and the corresponding mobilities in dependence of the field strength. The measured drift

velocity curve agrees well with other measurements [11,18–20].

The attenuation length λ is determined by multiplying the fitted attenuation time τ in eq. (1) with the known drift velocity. The attenuation length depends linearly on the field strength with the relation:

$$\lambda = \alpha \frac{E}{\rho}, \tag{3}$$

where λ is the attenuation length in cm, E is the electric field in kV/cm, ρ is the impurity concentration in ppm, and α is a constant determined to be (0.15 ± 0.03) cm^2 ppm/kV [21]. With this relation the impurity concentration (with oxygen as most important impurity) can be measured. For each run the impurity levels ρ determined at different field strengths agree within the errors. Fig. 8 shows the attenuation lengths in one run for different field strengths. The straight line is a fit to the data points. The line has to pass through the origin and the slope is directly the impurity concentration ρ. In a typical run a value of 0.15–0.3 ppb of oxygen equivalent was achieved. For the first runs the impurity concentration could clearly be seen to improve from run to run until the molecular sieves outgassed completely and small remaining leaks were fixed.

In a large scale detector long drift distances at moderate field strengths of about 1 kV/cm are important in order to keep the number of electronic channels small. As the attenuation length varies with the field, one can simulate long drift distances and long drift times by reducing the field. The longest observed drift times in the 10 cm chamber are of the order of 1.8 ms at 10 V/cm. This corresponds to impurities of about 0.2 ppb. With this value and eq. (3) an attenuation length of about 7.5 m is expected for a field of 1 kV/cm.

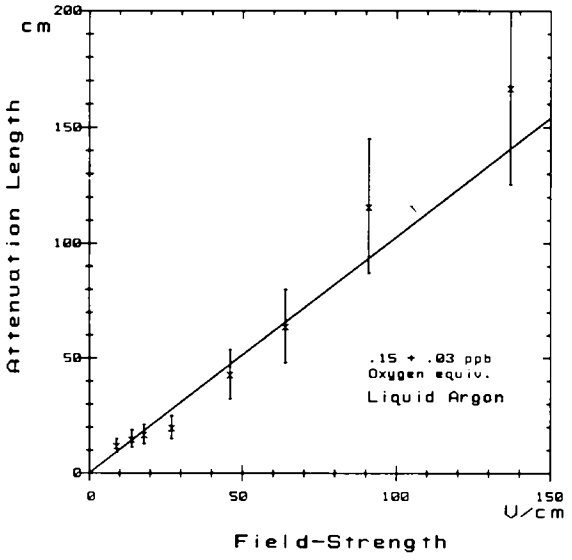

Fig. 8. Attenuation length in liquid argon versus drift field. The measurements are from one run.

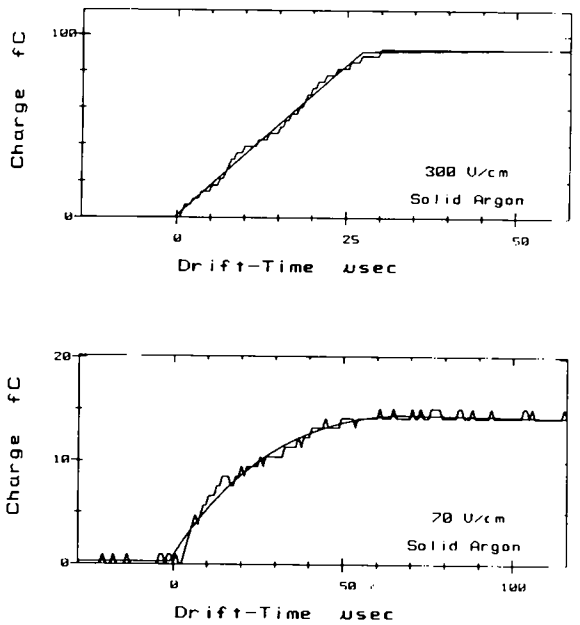

Fig. 9. Typical pulses in solid argon for field strengths of 300 and 70 V/cm. The fit of the expected pulse shape is superimposed to the measured pulse form.

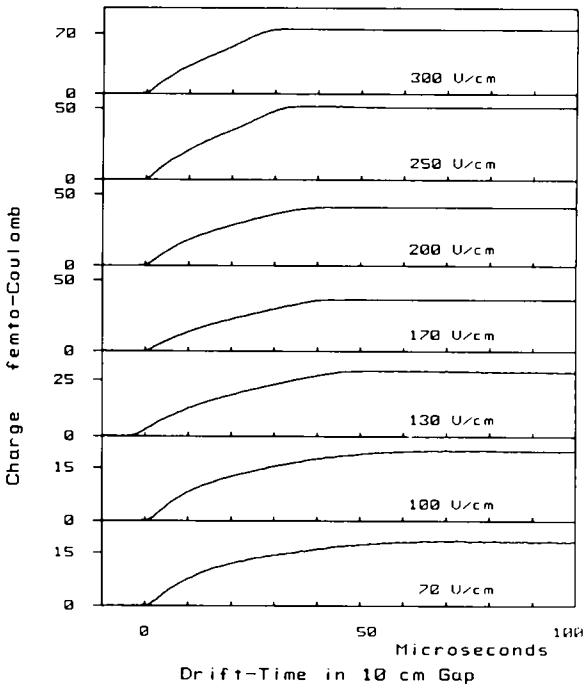

Fig. 10. Development of pulse shapes (average pulses) at different drift fields in the 10 cm chamber for solid argon.

7.2. Solid

The evaluation of the data in the solid argon follows the same principles as for the liquid. Much less information is available on drifting electrons over large distances and on the effects of impurities in solid argon. The drift velocity is strongly temperature dependent [11] within ten degrees around the melting point. Several measurements of the drift velocity can be found in the literature [11,20], but the agreement is poor.

The oxygen attachment coefficient in solid argon has not yet been measured and can be different from the value of the liquid phase. Thus the direct measurement of the impurity concentration of the solid argon was not possible. To overcome this difficulty the purity for each argon filling was determined in the liquid phase, where the attachment coefficient is known. The argon was then frozen and after several hours of data taking, the solid was melted at the end of each run and the measurements with the liquid were repeated. This was done to check that the impurity concentration did not vary considerably.

As for the liquid the pulses in solid argon can be described by eqs. (1) and (2) for the large and the small gap respectively. Fig. 9 shows two single pulses in solid argon for different field strengths with the fit superimposed. The development of the pulses for decreasing field strength can be followed in fig. 10 for the large gap and in fig. 11 for the small one. For the large gap it can be observed that the rounding of the pulses appears at higher fields than in the liquid.

The measured drift velocity in function of the electric field is shown in fig. 12. The data points agree for

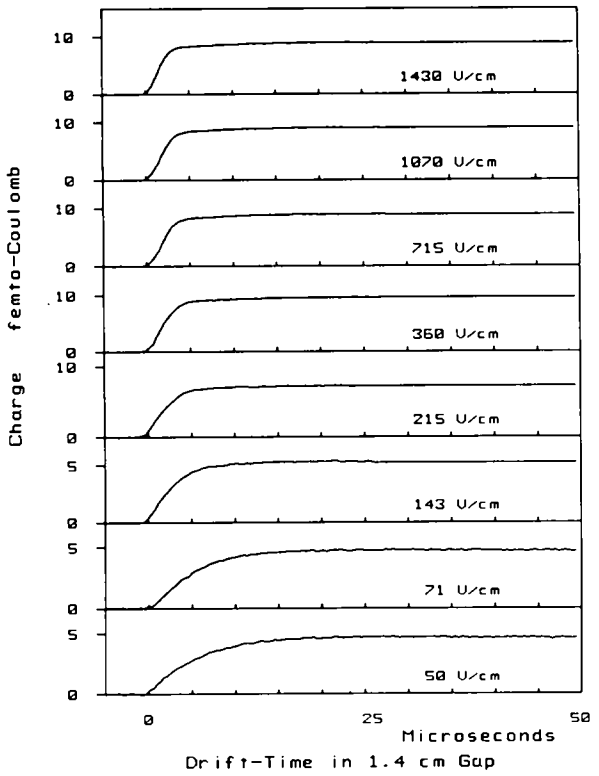

Fig. 11. Development of pulse shapes (average pulses) at different drift fields in the 1.4 cm chamber for solid argon.

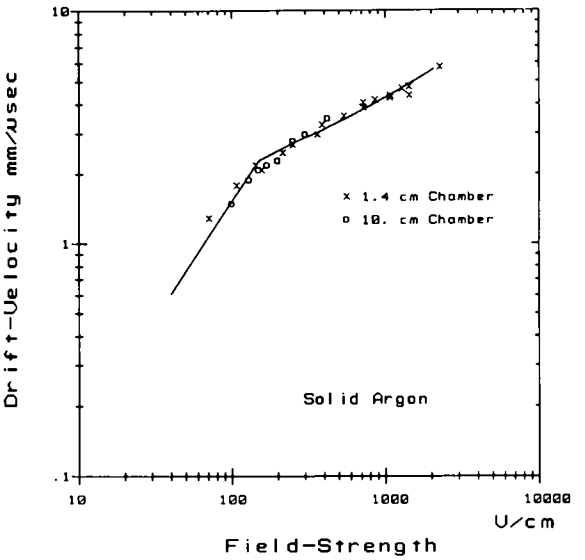

Fig. 12. Electron drift velocity in solid argon versus field strength. The open circles represent the data points measured with the 10 cm chamber. The crosses are measured with the 1.4 cm gap.

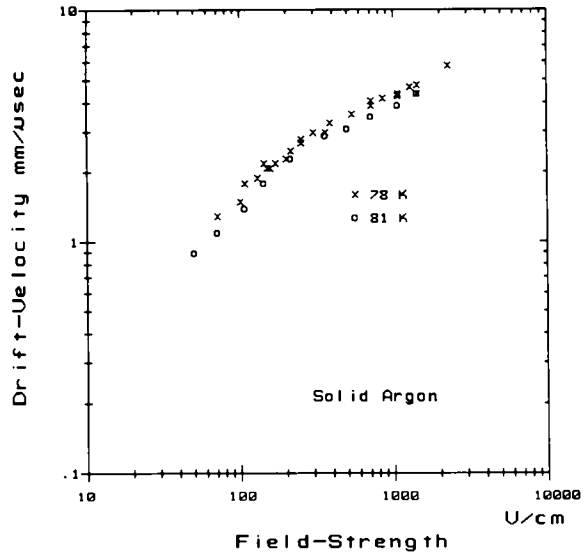

Fig. 13. Drift velocity in solid argon versus field strength at 78 and 81 K.

Table 2
Measured drift velocities in solid argon for the two temperatures in dependence of the electric field strength

E [V/cm]	v_d [mm/μs]	
	78 K	81 K
2270	5.8	
1430	4.6	4.4
1286	4.7	
1070	4.4	3.9
857	4.2	
715	4.0	3.5
536	3.6	
500		3.1
385	3.3	
360	3.0	2.9
300	3.0	
250	2.7	
215	2.5	2.3
170	2.2	
157	2.1	
150	2.1	
143	2.2	1.8
130	1.9	
107	1.8	1.4
100	1.5	
71	1.3	1.1

both the small and the large gap. They are also consistent through different runs, i.e. they are reproducible in different argon fillings. The electron mobility determined from the low field drift velocities is (1536 ± 170) $cm^2\ V^{-1}\ s^{-1}$. Thus the drift velocity in solid argon is nearly a factor of 3 larger than in liquid. The solid line in fig. 12 is a fit of the function $v_d = \mu_0 E$ for E less than 150 V/cm and an $E^{1/2}$ dependence above this value.

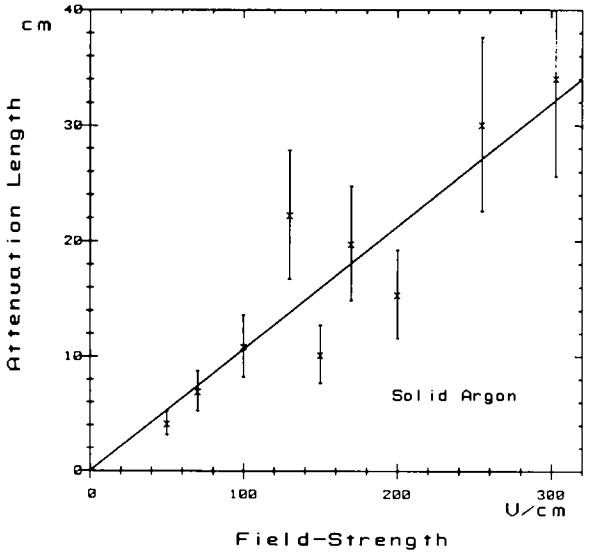

Fig. 14. Attenuation length in solid argon versus drift field. The measured points are from one typical run.

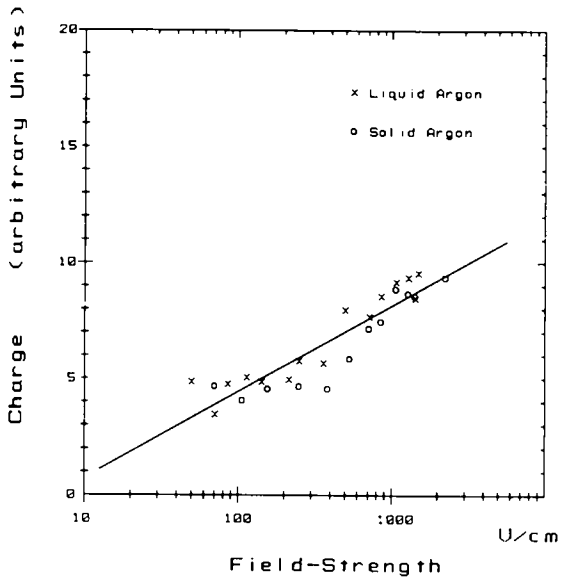

Fig. 15. Comparison of the charge output for liquid and solid argon for different electric field strengths.

To determine the influence of temperature on the drift velocity the chamber was cooled during one run by an argon–nitrogen mixture. The boiling point of this bath was 81 K instead of the 78 K of pure nitrogen. A systematic shift of the drift velocity versus field strength curve (fig. 13) of about 10% is detected. The measured values of the drift velocities for the two temperatures are listed in table 2.

With the known drift velocity the decay time of eq. (1) can be converted into the attenuation length. The attenuation length is plotted versus the electric field strength for one run in fig. 14. As for liquid argon the measured points lie on a straight line, but the slope is smaller. Thus the attachment to impurities seems to be much stronger in the solid. From the curve of fig. 14 an attenuation length of about 1 m can be extrapolated for a field strength of 1 kV/cm.

The charge output for liquid and solid argon is compared in fig. 15 for different field strengths. The errors on the single measured points are quite large, as can be seen from the spread of the curves, because the number of events per point was limited to about 100–150. Within these errors of about 20% the charge output is equal for both liquid and solid argon.

8. Conclusions

The study reported in this paper was initiated as a first step towards the realization of a large volume (2 kt)

liquid or solid argon image chamber [22] as underground detector for proton decay and solar neutrino physics. In this respect the results obtained appear extremely encouraging.

A very simple purification technique is capable of reducing the impurity level of the liquid to about 0.2 ppb oxygen equivalent, giving consistently very long drift paths of electrons. The expected attenuation length in liquid argon is 7.5 m at 1 kV/cm, i.e. larger than any drift-cell which seems practical. For solid argon an attenuation length of about 1 m is expected at 1 kV/cm. A detailed analysis of the ionization pulse shape was performed with a FADC readout, yielding direct information on both the purity level of the liquid and the electron drift velocity. Drift times as long as 1.8 ms in a drift field of 10 V/cm were observed in liquid argon. The operation of a large underground detector with frozen argon as sensitive medium seems possible and it is very appealing when one considers the advantages of the solid over the liquid, like the higher drift velocity, the fact that impurities cannot enter the frozen active volume and, even more important, the fact that the solid is much safer to operate with.

Acknowledgments

This work was supported by the US Department of Energy under contract number DE-AC02-76ER03064. The authors wish to acknowledge the excellent support received from the technical staff of the Harvard High Energy Physics Laboratory.

References

[1] R. Davis Jr., B.T. Cleveland and J.K. Rowley, in: Science Underground – 1982, eds., M.M. Nieto et al., AIP Conf. Proc. no. 96 (1983) 2.
[2] D.W. Swan, Proc. Phys. Soc. London 82 (1963) 74.
[3] C. Rubbia, CERN-EP Internal Report 77-8 (1977).
[4] W.A. Huffman, J.M. LoSecco and C. Rubbia, IEEE Trans. Nucl. Sci. NS-26 (1979) 64.
[5] H.H. Chen and J.F. Lathrop, Nucl. Instr. and Meth. 150 (1978) 585.
[6] H.H. Chen and P.J. Doe, IEEE Trans. Nucl. Sci. NS-28 (1981) 454.
[7] P.J. Doe, H.J. Mahler, H.H. Chen, Nucl. Instr. and Meth. 199 (1982) 639.
[8] K. Deiters et al., Nucl. Instr. and Meth. 180 (1981) 45.
[9] E. Gatti, S. Padovini, L. Quartapelle, N.F. Greenlaw and V. Radeka, BNL 23988 (Feb. 1978).
[10] J.H. Cobb and P.J. Miller, Nucl. Instr. and Meth. 141 (1977) 433.
[11] L.S. Miller, S. Howe and W.E. Spear, Phys. Rev. 166 (1968) 871.
[12] C. Rubbia, invited talk at the 4th ICOBAN Conf., Park City, Utah (January 1984).
[13] O. Bunemann, T.E. Cranshaw and J.A. Harvey, Can. J. Res. 27 (1949) 191.
[14] Messer Griesheim GmbH, Oxisorb Gas Purifying System.
[15] Union Carbide Corp., Linde Molecular Sieves 13X and 4A.
[16] Cajon Company, VCR Vacuum Couplings.
[17] J 310 by Siliconix Inc.
[18] B. Halpern, J. Lekner, S. Rice and R. Gomer, Phys. Rev. 156 (1967) 351.
[19] K. Yoshino, U. Sowada and W.F. Schmidt, Phys. Rev. 14 (1976) 438.
[20] E.M. Guschchin, A.A. Kruglov and I.M. Obodovskii, Zh. Eksp. Teor. Fiz. 82 (1982) 1114.
[21] W. Hofmann, U. Klein, M. Schulz, J. Spengler and D. Wegener, Nucl. Instr. and Meth. 135 (1976) 151.
[22] K.L. Giboni, Nucl. Instr. and Meth. 225 (1984) 579.